Article

Computational simulation of PT6A gas turbine engine operating with different blends of biodiesel: A transient-response analysis

Camilo Bayona-Roa [1,2], J.S. Solís-Chaves [1]* (iD) **Javier Bonilla[1] and Diego Castellanos [1]**

[1]   Laboratorio de Simulación Computacional - Universidad ECCI; jsolisc@ecci.edu.co
[2]   Centro de Ingeniería Avanzada, Investigación y Desarrollo – CIAID, Bogotá (Colombia); cbayonar@unal.edu.co
*   Correspondence: jsolisc@ecci.edu.co
‡   These authors contributed equally to this work.

Abstract: A computational simulation of a PT6A gas turbine engine operating at off-design conditions is described in the present article. The model consists of a 0-dimensional thermo-fluidic description of the engine by applying the mass, linear momentum, angular momentum, and energy balances in each engine's component. The transient behavior of the engine is simulated for different blends of the original JET-A1 fuel with bio-diesel. Simulated thermodynamic variables of the air at each engine's component, as well as some performance parameters correspond to the reported experimental measurements. The numerical results also demonstrate the ability of the computational simulation to predict acceptable fuel blends, such that the efficiency of the engine is maximized and its structural integrity is maintained.

Keywords: Gas turbine engine; Thermo-fluidic model; System dynamics; Bio-diesel; Thermal efficiency.

---

1. Introduction

The necessary thrust that is required for an aircraft to provide lift is commonly supplied by a heat engine. In particular, a gas turbine engine has the ability to convert heat energy into mechanical energy by involving the flow of air passing through several thermo-fluidic processes within its components. The most important feature of gas turbine engines is that, contrary to reciprocating engines, separate sections of the engine are devoted to the intake, compression, combustion, power conversion, and exhaust processes. This also means that all processes are performed simultaneously and are strongly coupled between them.

Various levels of modeling of operational gas turbine engines, ranging from the systematic engine simulation in [1–6], to the detailed component manufacturing of engine parts in [7–9] rely on the thermo-fluidic modeling of each engine's component. In this sense, as the engine's model increase in detail it may lack maturity and robustness: detailed models are based on *Computational Fluid Dynamics* (CFD), which describes numerically the air flow through the components of the engine, including the combustion phenomena inside the burner. But fully three-dimensional CFD models resolve separately the thermo-fluidic phenomena occurring at each engine's component [10,11]. Those models are mostly devoted to the design of the turbo-machinery components of the engine (e.g. compressor's and turbine's blades), rather than providing the full operational response. Indeed, the aerodynamic matching of stages within the turbo-machinery, and even worst, it's coupling with other physical descriptions such as the combustion or the blade dynamics, greatly impedes the utility of these models.

This article aims to computationally simulate a gas turbine engine when operational parameters like the fuel type are modified. We develop a computational simulation -in the sense of the *System Dynamics* (SD) analysis- which is capable of giving the transient response of the gas turbine engine's performance when a change in the operation parameters occurs. Specifically, when the Jet-A1 fuel that is typically used is replaced by a blend with bio-diesel. We rely on the wide range of thermo-fluidic models that have been proposed in the literature: from

systematic models in [12–14], to detailed mathematical descriptions in [15–17]. But the conceptual description of the gas turbine engine's response is complex; it involves the approximation from very different engineering disciplines: Aerodynamics, Thermodynamics, Heat Transfer, Structural Analysis, Materials Science and Mechanical Design, among others. As the main objective of this work is to provide predictive information about the engine operation at off-design conditions, including the computational simulation of test bench analyses and the complete monitoring of the engine, we implement a model that gives a systematic response of the gas turbine engine. This model is aimed to give the indication of the various sensors -Avionics- in the engine. For example, the pressure and temperature of the air stream and the rotating power of the shafts occurring at the different stages of the engine's components.

We restrict our survey to computational codes that give the avionics response of the engine: applications can be found in the literature ranging from preliminary analysis of the new system's designs, like the ones described in [18–20], to detailed responses of each component's settings in [21–23]. These fast computational-based engine simulations are the milestone to prevent *in-flight* operational failures *on-live*, when engine's parameters are modified. Our model focus on describing the primary flow-path components such that on-live calculations can be achieved, and avoids the description of the structural behavior of the solid parts of the engine, which are not essential in the engine's operation. Since some other non-flow-path components affect the ability to maintain the operation conditions, accounting for them can be significant to obtain accurate simulations. This is the case of the combustion control system or the external loads related to the propeller. In any case, the excluded relationships from the model are the engine-inlet or engine-outlet integration (to reproduce the inlet and outlet flows), the engine-aircraft integration (to reproduce structural analysis), the engine-environment integration (for adverse weather and pollution), and the control systems.

The remaining parts of this article are organized in the following order. In Section 2 the real operational gas turbine engine is described: we reproduce a generic version of the Pratt-Whitney PT6A engine. Simultaneously, we present the theoretical description of the thermodynamic processes occurring inside each engine's components and the SD approach. The simulation of different operation scenarios are given in Section 3. The scenarios include a benchmark problem of the engine's steady operation using Jet-A1 fuel, the subsequent operation with blends of bio-diesel, and the transient engine response at the start-up procedure. Finally, in Section 4 some conclusions close the article.

2. The PT6A engine model

A generic version of the Pratt-Whitney PT6A "Medium" engine, including the labeling of its parts, is displayed in Fig. 1. In general, gas turbine engines consist of: an air inlet, a compression section (including the compressor and diffuser), a combustion section (combustion chamber), a turbine section, an exhaust section, and an accessory section (for necessary systems). The theoretical description of the thermodynamic processes occurring in these components is Brayton's cycle. But the dynamic simulation of the engine's behavior must account for non-equilibrium conditions, which is the case of the start-up procedure of the engine. The Brayton's model must, therefore, be complemented with the actual design of the turbo-machinery of the engine's stages.

We develop a gas-dynamical model for describing the thermo-fluidic phenomena present in each gas turbine engine's component. For doing so, we apply the fluid's continuity balance for each component with transient mass storage, namely the combustion chamber where compressible effects of the air are relevant, and for the coupling of mass fluxes between consecutive components. We also apply the fluid's momentum balance at the core flows in the compressor and turbine stages. Fluid's energy balance accounts for the combustion chamber heat addition and for the compression and expansion processes. The mechanical energy equation is also applied to the rotor stages, including the inertial term of the rotor shaft, in order to model the mechanical coupling between the moving components. The application of these balances to the engine's components results in a *0-dimensional model* representing the operation at transient state. The model is usually confined to the normal operating range of the engine, but in the present work is aimed to give a response to a change in the operational conditions of the engine.

A practical approach to solve the 0-dimensional model is to implement it in SIMULINK® software [24], which possess a graphical user interface for building algebraic *block diagrams* that define the governing differential equations. Hence, we present the block diagram of the governing equations in Fig. 2, where the engine model is represented at a component level. An extended explanation of each engine's component, and how we represent it, is developed in the

following paragraphs. Moreover, each component's block diagram will be presented through the detailed explanation of each sub-system. We list inputs, parameters, variables, and outputs for each block diagram.
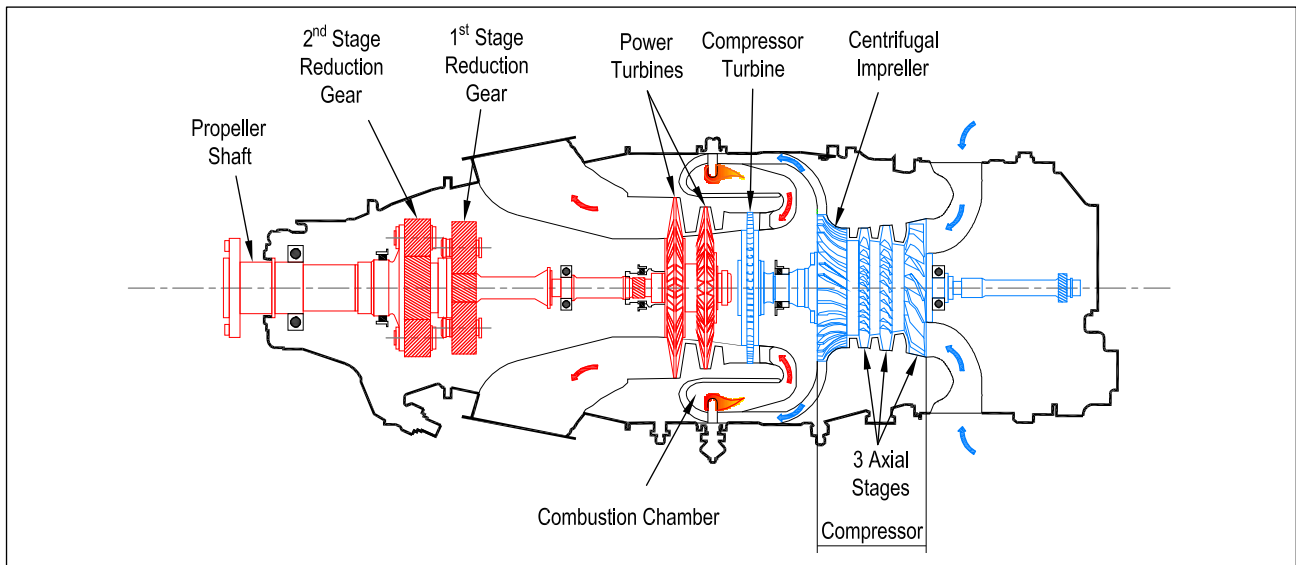
Figure 1. Cross section of the Pratt-Whitney PT6A engine.

2.1. Air inlet

One of the main characteristics of this gas turbine engine is that in most aircraft installations it is mounted backward in the nacelle. This feature makes that the airflow inside the components of the engine is directed in the same direction as the aircraft's displacement. Another consequence is that the intake is located at the rear part of the engine, and therefore, the air passes through the exterior of the aircraft (and the engine itself) before entering to the intake. The PT6A design cares for guiding the intake air to the engine using ducts that avoid facing the exhaust gases: since the typical requirement is to provide laminar air into the compressor -so that, it can operate at maximum efficiency-, the inlet duct changes smoothly from opposing the direction of the airflow to the axially forward direction of the aircraft's speed.

We define the inlet component as to be the intake air conditioner: even though our model is restricted to an on-ground operation, with no rarefying processes of the atmospheric air entering into the engine, we extend the possibility of the operation of the model during *in-flight operation* conditions. This effect is modeled using the relations for the pressure and temperature of the air which are presented in the block diagram of Figure 3. In the model, p_{atm}, and T_{atm} are the atmospheric pressure and temperature, $M = u/c$ is the flight Mach number that relates the aircraft speed u with the speed of sound $c = \sqrt{\gamma p_{atm}/\rho}$, γ is the quotient between specific heats of the air, and η is the isentropic efficiency. We use the subscript 1 to label the thermodynamic variables of air at the inlet. Note that when the engine is supposed to operate in the *test bench*, the model equates the inlet conditions to the atmospheric conditions $p_1 = p_{atm}$, and $T_1 = T_{atm}$.

2.2. Compression section

In the PT6A gas turbine engine (used for aviation), the compression section consists of three *axial stages* and a single *centrifugal stage*, each considered to be a rise in the air's pressure: the air flows from the inlet duct to the low-pressure compressor, and then to the next two axial flow stages before passing to the centrifugal stage. The axial stages are composed by rotating blades called *rotors*, and static blades called *stators*. Those rotating stages move at around 40000 Revolutions Per Minute (RPM) increasing the air's pressure more than eight times the inlet's pressure. The last stage of the compressor section is composed of a single centrifugal-flow compressor that accelerates the air outwardly. This centrifugal section has a high-pressure rise, but since there can be several losses between centrifugal
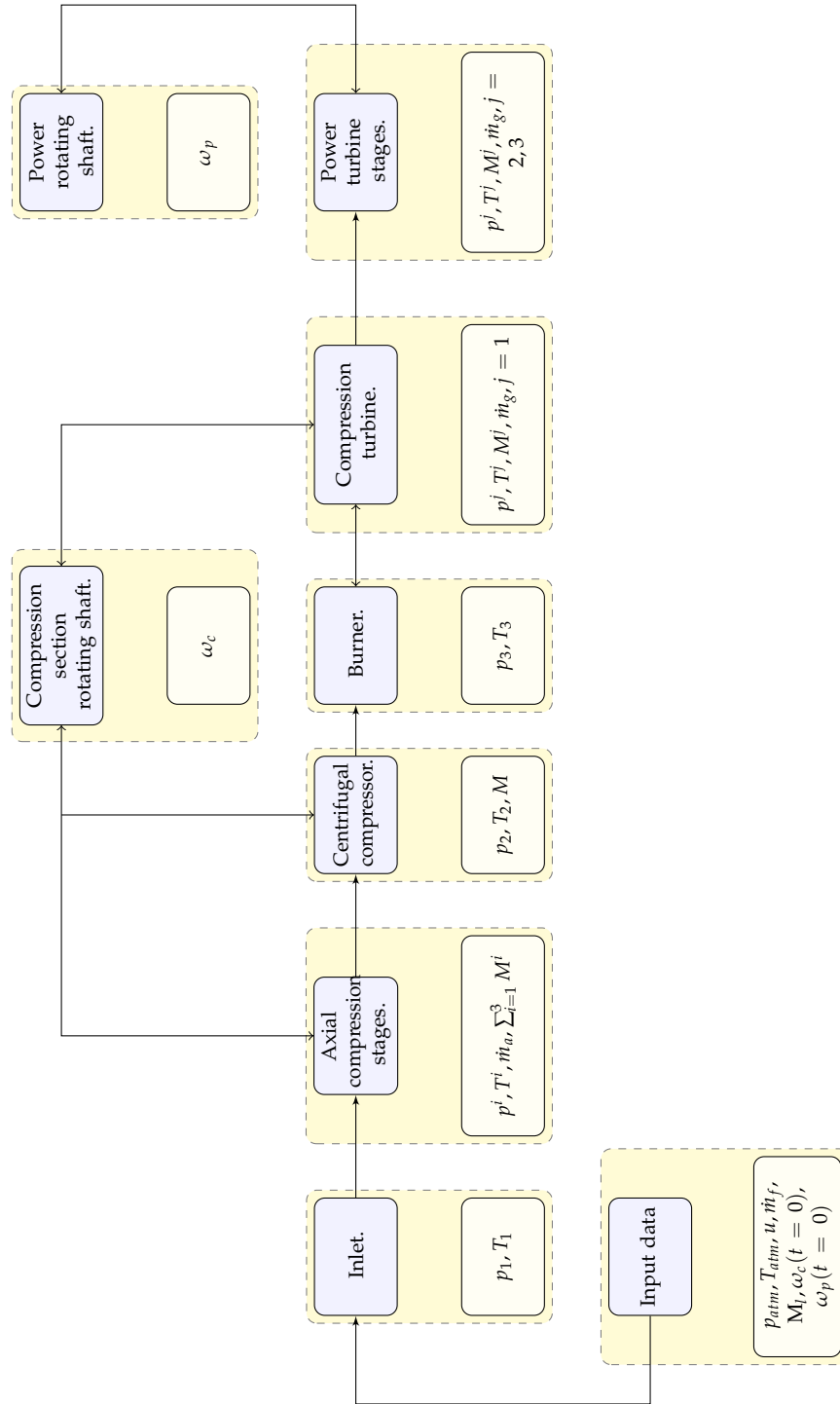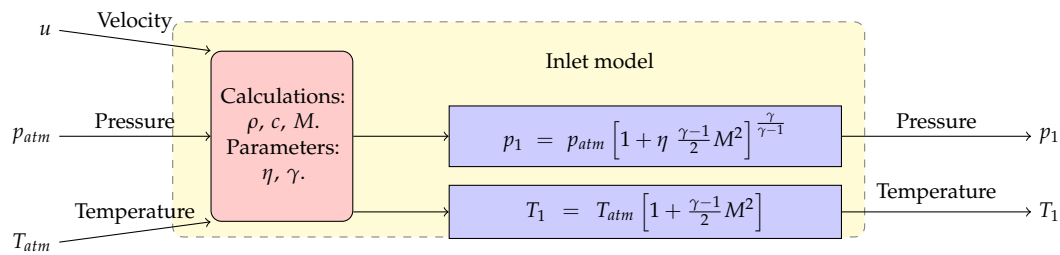
Figure 2. Flow chart of the PT6A engine's model.

Figure 3. Inlet model.

stages, it is restricted to a single stage before discharging the airflow. The air stream then leaves the centrifugal compressor section via the diffuser, which is a section of the engine just before the combustion chamber that has the function of preparing the air for the burning area so that it can burn uniformly and continuously. We neglect the diffuser in our representation of the compression section of the engine.

A work previous to the modeling of the compressor has to do with the estimation of its geometry. In this sense, we determine the compressor's geometry by extracting most of the information from technical reports, as well as from the engine's manual Whitney [25]. Since the axial compression section geometry has been reported in [26] for a four-axial stages PT6A engine, we transcript the geometrical parameters for the first and last stages, but calculate the mean values of the second and third stages of that compressor, and set those values as the second axial stage of our PT6A axial compressor model. The geometric parameters that we have processed for each axial stage geometry are presented in Table 1. In the case of the inner and external radius of the rotor blades, we determine those parameters from cross-checking the engine's manual schemes and the measured values from a disassembled engine. The geometry of the centrifugal compressor is described the rotor's blade geometry and the inlet's and outlet's cross-sectional dimensions, where the inner r_1 and outer r_2 radii of the rotor are determined from the engine's technical report, being 92 mm and 117 mm, respectively.

Blade	Symbol	1st-stage rotor	2nd-stage rotor	3th-stage rotor
Inlet air angle, deg.	α_l	61.5	59.8	58.0
Exit air angle, deg.	α_t	54.4	48.9	42.0
Inlet metal angle, deg	β_l	56.8	57.85	57.1
Exit metal angle, deg.	β_t	50.5	43.5	36.2
Inner radius, mm.	r_0	72	76	80
Outter radius, mm.	r	100	96	92

Table 1. Processed values of aerodynamic and geometric parameters for the axial compressor stages.

The overall compression stage is defined from the compressor intake (p_1, T_1) to state 2, at the diffuser outlet (p_2, T_2). Therefore, it covers the three axial stages, the centrifugal stage, and the diffuser of the PT6A engine. Knowledge of the inlet (upwind) conditions of the air, such as temperature and pressure, as well as the rotational speed of the engine's rotating shaft, is required. Also, the knowledge of the geometry of the compressor at each stage is mandatory to apply the continuity, momentum and energy balances on which the enthalpy raise and the mass flow depend. Since each compression section is composed of successive stages of rotating blades (rotors) and stationary guide vanes (stators), we analyze at each rotor-stator stage the transmission of the shaft's mechanical energy into the air's fluid energy and compose the complete compressor performance by adding the multiple successive compression stages.

For simplicity, we assume that the compressor's blades are thin, rather than having the complete airfoil cross-shape geometry. This supposition is acceptable since in the PT6A engine those are constructed of sheet metal. In the case of the axial compressor, we analyze a single $i-$th stage, where a rotor precedes a stator, and consider the same hub radius for the rotor as for the stator. We also make this supposition for the shaft radius at each axial stage. Nevertheless, we consider different cross areas between consecutive compression stages, such that the axial component of velocity can be calculated to conserve mass: in the case of the multistage axial-flow compressor, the blades of each successive stage of the compressor get smaller as the air gets further compressed. In each rotor-stator stage, we consider the cross section of only one stator and rotor blade as it moves vertically, knowing that the next rotor blade passes shortly

141 thereafter. This is the well-known cascade two-dimensional approximation of turbomachinery analysis, and which
142 configures our control volume.

143   We aim to calculate the variation in the air's velocity originated by the rotor's torque. To do this, we apply a
144 simplified analysis of the fluid's dynamics of the air occurring through the blade: the *velocity triangle*. The axial speed
145 of the airflow v_a^i can be measured at the inlet section, such that the volume flow rate can be calculated in terms of the
146 cross-sectional area. Another possibility is to know the inlet air angle (presented in table 1), such that the axial velocity
147 is calculated from the velocity triangle. To evaluate the torque on the rotating shaft, we use the angular momentum
148 balance that states that the total momentum in the shaft M is equal to the change between the angular momentum of
149 the flow that crosses the surfaces of the control volume. This change is only related to the tangential velocities of the
150 air given by the velocity triangle analysis.

151   In our model, we consider reversible losses in the compression stages, and therefore, full mechanical efficiency.
152 This implies that the shaft power is the same as the power delivered to the air. We suppose a quasi-static process in
153 which the difference between the amount of energy in the air is given by the increment in power and calculate the
154 temperature rise inside the axial compression stage by applying the energy balance in the control volume. We suppose
155 then, that the net pressure head induced by the compressor is modeled as a polytropic process, where the pressure
156 ratio Π is related with the temperature variation of the air and the polytropic constant of the gas n. The previous
157 exposition is concisely presented in the block diagrams of Figures 4 and 5.

158   In the case of the centrifugal compressor, we consider that the circumferential cross-sectional area can be defined
159 by the radius and the width of the blade b. For completeness, we suppose that the flow is defined completely in
160 the normal direction $(v_1)_n$, and therefore, the normal velocity at the outlet of the blade can be calculated with the
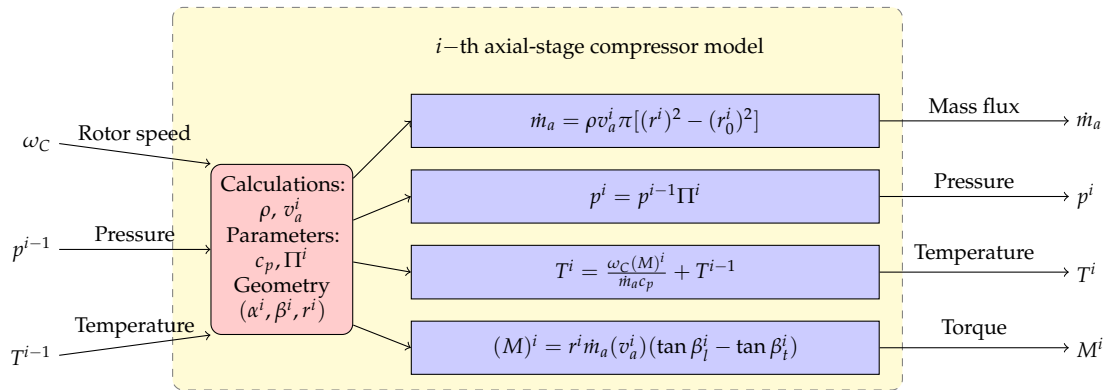161 conservation of mass.
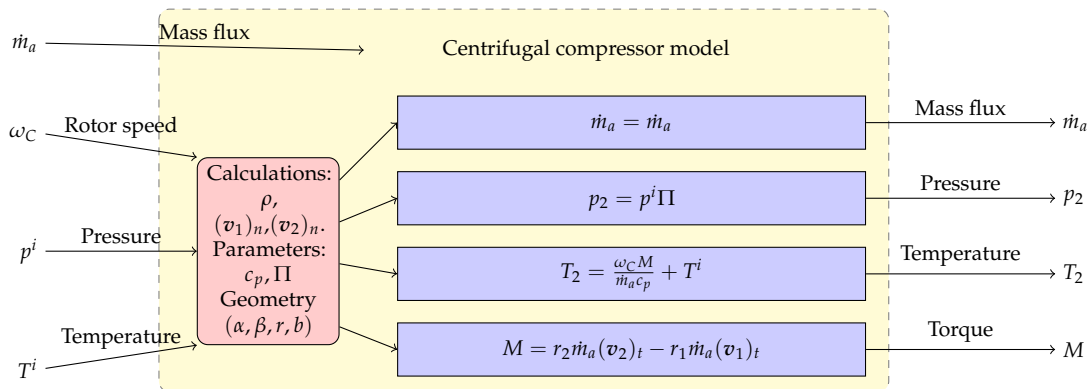

Figure 4. Axial stages compressor model.

Figure 5. Centrifugal compressor model.

2.3. Burner

The PT6A burner is mainly characterized by the split in the amount of compressed air that is used for maintaining the combustion: only a fraction of the air entering in the burner reacts with the fuel, while most of the compressed air is used for cooling purposes. The geometrical shape of the burner chamber is an annulus. In this sense, the overall volume is hard to be determined and we have approximated its value from measurements of the disassembled engine's burner to be around 0.028 m^3.

Inside the burner, the fuel and the air are separated apart before the flame: combustion with the liquid fuel is performed by the injection of the fuel inside the air stream. Scattering of the fluid into fine droplets leads to the convection and final evaporation of the liquid inside the compressed air-stream. This mixture is a steady non-premixed stream of air-fuel before the full combustion reaction takes place inside the burner. Buoyant mechanisms, but mostly forced convection and turbulence mechanisms of inlet air (due to its high pressure and temperature at the exit of the compression section) maintain the combustion process in the flame. The reaction rate and the products of the combustion (exhaust gases) depend on the quality of the air-fuel mixture occurring before the flame.

The combustion quality is automatically controlled by the *combustion control system* that fixes the amount of injection of fuel; this control is set by default for the Jet-A1 fuel. We neglect the combustion control in our present approach since we aim to investigate the response of the engine to different blends with biodiesel. The change in the physical properties of the fuel affects its spraying as it passes through the fuel injectors in the combustion chamber. This has effects on the maximum temperature inside the fuel chamber at the start-up of the engine. In this sense, the starting procedure has to be designed to be rigorous and must be established for each new operating fuel. For all the above, computational simulation of the particular gas turbine engine's performance is proposed as a predictive tool for the engine operation, which allows determining the operation variables when the change in the composition of the fuel occurs. This, with a low cost, and without risking the operation of test engines.

Our approach to model the burner's combustion phenomena is simple. The net power of the gas turbine engine is related to the amount of fuel that is burned inside the burner: the heat added to the air-stream is calculated from the energy balance inside the burning chamber, where LHV is the Low Heating Value of the fuel that represents the amount of energy that is delivered in the combustion process (accounting for the steam boiling in the liquid fuel). This is depicted in the block diagram of Figure 6.

Note that the amount of chemical energy that is transferred to the air (which is later transformed to mechanical energy in the turbine) depends on the type of fuel used, and this is completely characterized by the fuel flow rate and its lower heating value. The burner also works as an accumulator of mass, where the temporal change of the thermodynamic conditions of the air inside the burner is related to the amount of fuel $\dot{m}_f$, the incoming air flow rate $\dot{m}_a$, the exhausting rate flow of gasses $\dot{m}_g$, and the volume of the chamber V_B. Nevertheless, we describe the temporal variation of the pressure inside the burner to be solely represented by a loss of pressure (with coefficient $C_b \leq 1$).
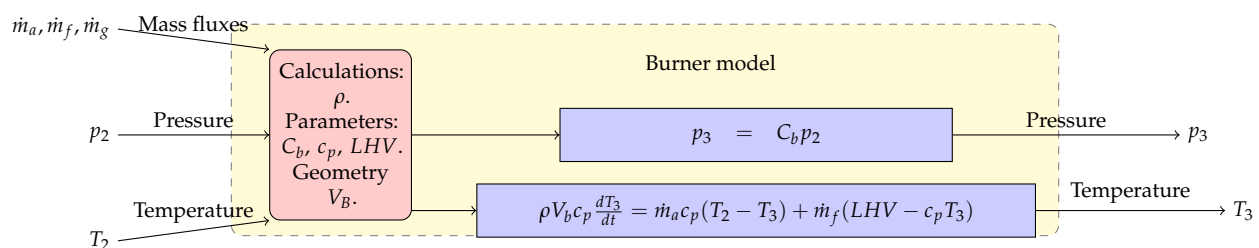

Figure 6. Burner model.

2.4. Turbine section

The air stream leaves the burner with the addition of heat from the combustion and flows through several turbine stages. The first turbine stage is a single-stage axial turbine that powers the compression section synchronously rotating at 40000 RPM via the *engine spool*, or common shaft. We determine from measurements of the disassembled engine spool an overall mass moment of inertia of the engine spool of about 0.12 Kg m^2.

200 In the PT6A, the hot air flows then into the *power turbines*, which are composed by two axial stages that turn at
201 about 30000 RPM, and that are connected to the main shaft that drives the propeller (or load). We also determine that
202 the mass moment of inertia of the main shaft is 0.06 Kg m^2. The air is discharged next to the exhaust, and then to the
203 atmosphere, where the air recovers its original free-stream conditions.

204 The turbine process is defined from the state 3 at the combustion chamber outlet (p_3, T_3) to state 4, at the engine
205 outlet (p_4, T_4). This means that the expansion ratio of the gas is known for the turbine section. Indeed, knowing the
206 expansion ratio of the $j-$th stage Π^j, one can model each turbine stage as a polytropic expansion process where the
207 pressure and temperature of the air at the discharge can be calculated straightforward.

208 The temperature drop is used then to calculate the retrieved mechanical power inside the turbine. Again, we
209 suppose a complete transformation efficiency between the fluidic and the mechanical power, such that the extracted
210 torque at each axial stage of the turbine is equal to the change in the angular momentum of the air inside the turbine.
211 Similarly to the axial flow compressor analysis, an accurate model of the turbine performance can be derived from a
212 detailed computation of the aerodynamics of the flow over the individual blade elements. The distinctive feature of
213 the turbine is that the mass flow rate of gases through the turbine section depends on the expansion work: we use the
214 angular momentum balance in order to obtain the mass flow of gases through the turbine stage, and therefore, the
215 axial term of the air velocity. The turbine relations are presented in the block diagrams of Figures 7 and 8.
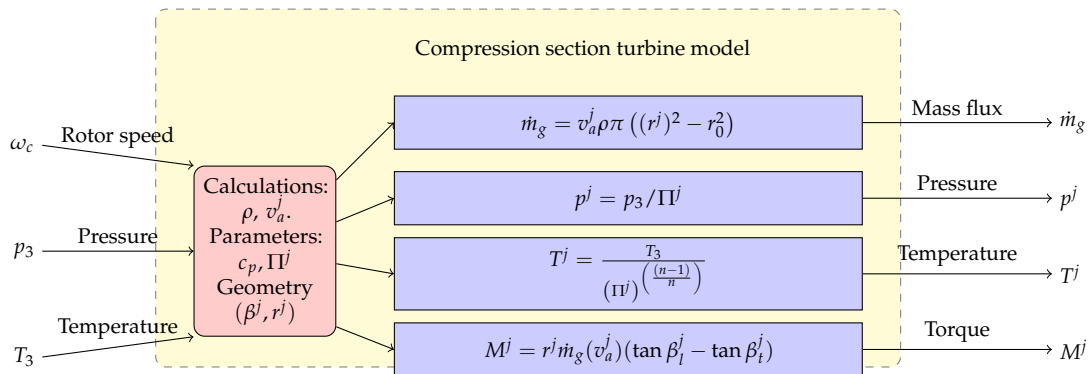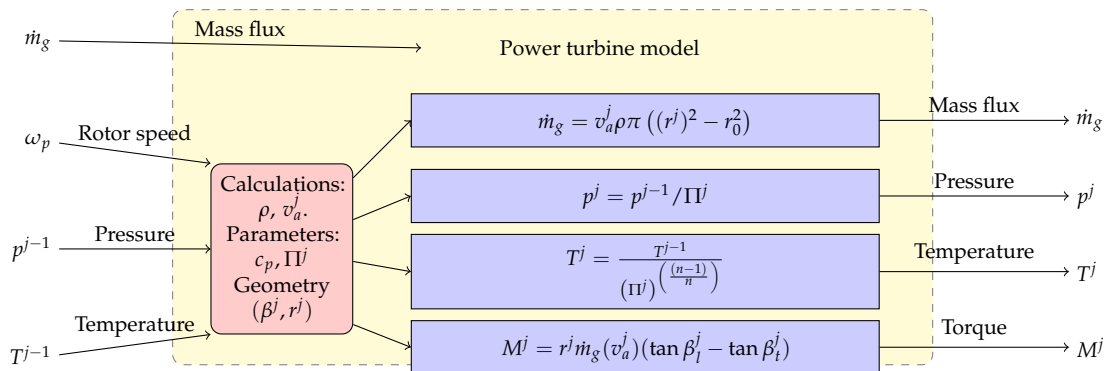

Figure 7. Compression section turbine model.

Figure 8. Power turbine model.

2.5. Rotating Shafts

217 The rotating shafts are modeled by applying the balance of angular momentum. We use the rigid body assumption,
218 and apply the momentum balance in the rotational motion, such that the acceleration power of the shaft must equal
219 the balance between turbine power, compression (or load) power, and parasitic powers. The angular momentum
220 balance applied to the engine spool, as well as the power rotating shaft is presented in the block diagrams of Figures 9
221 and 10. We define I_R to be the mass moment of inertia of the rotating shaft about its rotating axis, $\boldsymbol{M}$ is each one of the
222 torques applied to the shaft, and ω is the angular velocity of the shaft which can be calculated in terms of $\omega = N\pi/60$,

223 being N the revolutions per minute. We assume a parasitic power from the friction of the rotating shaft. The parasitic
224 torque M_f can be modeled as a bearing friction coefficient b that multiplies the rotational speed, with its effect acting
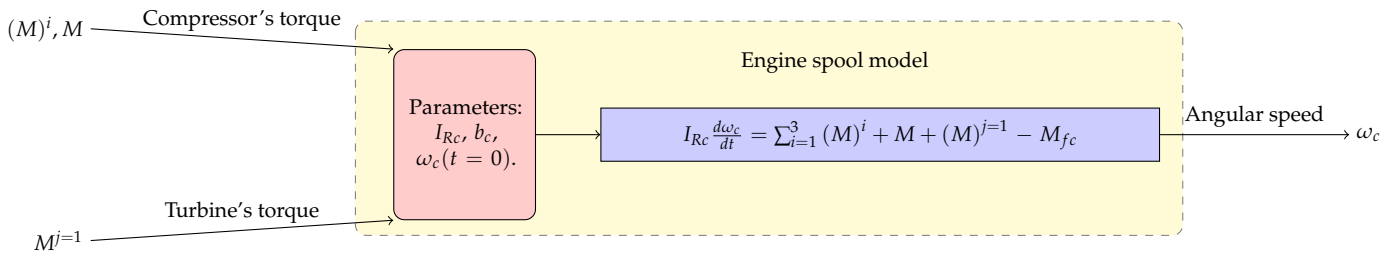225 in the contrary-rotation sense.

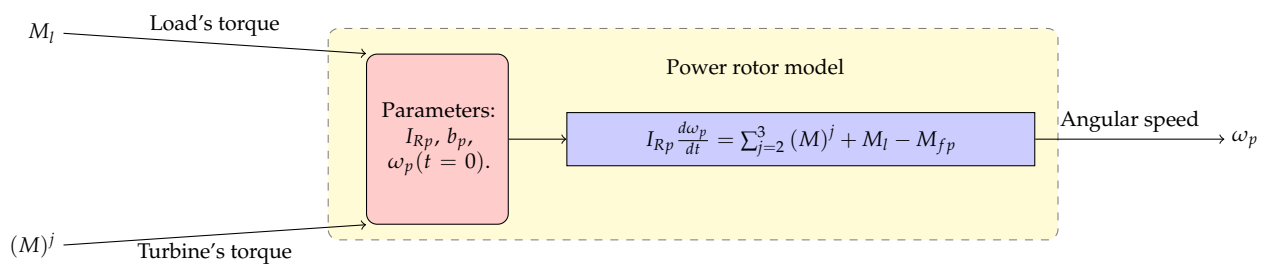

Figure 9. Compression section rotor shaft model.

Figure 10. Power turbines rotor model.

2.6. Compatibility conditions

227 Besides the physical description of each engine's component, one must close the engine's model coupling the
228 different components to what is referred to the *compatibility conditions*.

229 The mass compatibility conditions are related to the conservation of the air mass flow rate. The inlet's air mass
230 flow rate $\dot{m}_a$ is calculated by knowing the inlet air angle at the first axial stage, such that the axial velocity can be
231 calculated knowing the rotational speed and the geometric parameters of the rotor blades. It has been explained
232 that $\dot{m}_a$ is conserved among the stages of the compression section. Nevertheless, the mass compatibility condition
233 differs substantially when the air enters the burner: the exhaust gasses mass flow rate $\dot{m}_g$ is not only related to the
234 compressed air flow $\dot{m}_a$ reacting with the mass flow of fuel $\dot{m}_f$, but the exhaust gasses depend on the flow through the
235 turbine section and the engine's exhaust. Here the compatibility condition is related to the mass flow rate resulting
236 from each turbine stage. Some further explanation about this compatibility condition will be taken in the next section.

237 On the other hand, the angular momentum compatibility condition is the balance of the torques applied for each
238 rotating shaft. Its readily understood that the rotation speed of the axial and centrifugal compressor stages matches
239 with the compressor's turbine via the engine spool. In the same line, the velocity of the power turbines rotating shaft
240 matches the propeller's shaft velocity through the reduction gear.

241 Finally, the energetic compatibility conditions are associated with the thermodynamic variables of the air at each
242 one of the stages of the engine. It has been readily mentioned that the air enters each consecutive stage with the
243 pressure and temperature conditions that it obtains at the stage immediately before. This is clear from the overall
244 system's block diagram depicted in Figure 2.

3. Numerical Results

246 In this section, we present the numerical results for several different simulation scenarios. The first scenario is the
247 steady response of the engine which is intended to validate the computational model. Then, we solve the steady-state
248 operation by using the blends with biodiesel. Finally, we address the transient operation of the engine using the fuel
249 blends, specifically at the start-up of the engine, when the maximum temperatures can be reached. We suppose an
250 on-ground operation in all scenarios so that the inlet velocity is set to zero.

Table 2. On-ground steady operation conditions using Jet-A1 fuel. Extracted from [25].

Standard conditions	Value
Atmospheric temperature	288 K
Atmospheric pressure	101352.9 pa
LHV of Jet-A1 fuel	42.8 MJ/Kg
Jet-A1 fuel mass flow	0.062 Kg/s
Propeller's load (at propeller's shaft)	2684.51 N.m

3.1. Validation of the computational model

We first validate the computational model by considering a standard operation of the PT6A engine reported in the operation manual [25]. The geometrical parameters of the PT6A motor are implemented in the computational model correspondingly to Section 2. The operation parameters are presented in Table 2, where the International Standard Atmosphere (ISA) conditions are set as the environmental conditions. We also assume a constant flow of Jet-A1 fuel, with a calorific power of 42.8 MJ/Kg, and a constant propeller's load of 2684.51 N.m. We evaluate the stationary response of some tracked variables (invariant in time): for the sake of validation, we track the stationary pressure, temperature and air flow at the stations of the engine. We also set the polytropic constant of the air to $n = 1.4$, and fit some remaining geometric parameters of the model so that we obtain the closest numerical results to the ones reported in the operation manual. In Table 3 we list the experimental results that have been previously reported in the operation manual for several stations of the engine, and that we use for the sake of comparisons.

We first determine the compression and expansion ratios based on the experimental measurements. The overall compression ratio at the axial stages can be calculated from the data in Table 3 to be 3.14 : 1 atm, while for the centrifugal compressor the compression ratio is around 2.56 : 1 atm. In this sense, we fit the centrifugal compressor's angles β_1 and β_2 to 40 and 38 degrees, respectively, such that the centrifugal compressor gives rise to the pressure change. On the other hand, the expansion ratio for the compression and power turbines are calculated to be 1 : 3.03 atm and 1 : 2.18 atm, respectively. We suppose an expansion ratio of 1 : 1.47 atm for each stage of the power turbines section, and fit the blade's angles in order to fulfill the mass flow rate compatibility (conservation) condition between the different turbine stages. Table 4 presents the fitted aerodynamic and geometric parameters for all the turbine stages of the PT6A engine that have been processed. These parameters have been determined following the previously exposed ideas, from cross-checking the engine's manual schemes and the measured values from a disassembled engine, but mostly from the fulfillment of the mass conservation requirement. The rotor blade airfoils, which are metal profiles followed and preceded by stator vanes, are completely defined by these geometric parameters. Finally, the parasitic power that is lost due to friction can be modeled by setting the bearing coefficients b_c and b_p to 0.04 Kg.m^2/s and 0.05 Kg.m^2/s, respectively, for the engine spool and power rotor shaft. We also model the pressure loss coefficient in the burner to be $C_b = 0.95$.

The simulated steady engine response is presented in Table 5. In that table, we list the temperature and pressure along the stations of the PT6A engine, together with the calculated relative error against the experimental measurements. We confirm a consistent physical behavior of those thermodynamic variables. Distinctively, the observed pressure at the discharge of the axial compressor stages is higher than the reported one. This inaccuracy is countered by the centrifugal compression section, where the blade's geometrical parameters are fitted to give accurate results of the overall compression ratio. In this regard, fitting the compressor's parameters affects negatively the accuracy of the temperature at the discharge of the compression stage, but the energy balance inside the combustion chamber counteracts this effect, and matches the stipulated temperature in the manual, with an error of only 1.57%. Temperature and pressure variables at the expansion stages correspond well to the experimental counterparts, mainly due to the possibility of fixing the expansion relation and the geometrical parameters of the turbines. Given the previous exposition, we believe that the error is restricted to a low range such that it validates the usage of the proposed model for predicting the engine response when new operating conditions are evaluated.

3.2. Stationary operation of the PT6A using fuel blends

Once the computational model has been validated, the following simulation scenarios are considered: we evaluate the stationary operation of the PT6A-42 engine at both 100% of the fuel mass flow and 60% of the fuel flow, meaning

Table 3. Temperatures and pressures for PT6A-42 engine at 850 shp and ISA standard conditions. Extracted from [25].

Station	Location	Temperature (K)	Pressure (pa)
0	Ambient	288	101352.9
1	Compressor Inlet	288.2	102042.4
1.5	Interstage Compressor	415.4	307506.2
2	Compressor Discharge	610.4	787381.28
3	Turbine	1212.1	770144.39
3.5	Inter Turbine	967.1	246142.8
4	Turbine Exit	811.5	113074
5	Exhaust	811.5	106179.3

Table 4. Fitted aerodynamic and geometric parameters of the turbine stages.

Blade	1st-stage rotor	2nd-stage rotor	3th-stage rotor
Inlet metal angle, deg	-20	-20	-20
Exit metal angle, deg.	80	43	43
Inner radius, mm.	92	90	88
Outter radius, mm.	117	125	142

two different engine operation throttles. Since we aim to predict the engine's response to the usage of new hypothetical fuels, we vary the parameters that represent the fuel and perform the simulation. In this sense, the standard Jet-A1 fuel is mainly composed of $n-$heptane and isooctane, which are hydrocarbons that possess between 8 and 16 carbon atoms per molecule, giving a LHV of around 42.8 MJ/Kg (measured in experimental tests [27]). On the other hand, the chemical composition of a biodiesel sample results in an approximated LHV value of 36.29 MJ/Kg [28]. Hence, the pure biodiesel retains a smaller amount of energy than conventional Jet-A1 fuel. We simulate the operation with biodiesel fuel, as well as other hypothetical blends of Jet-A1 with biodiesel. In this sense, we establish a discrete range of mass concentrations of biodiesel in Jet-A1 which are 3 in total: 10% of biodiesel (B10), 20% of biodiesel (B20), and 30% of biodiesel (B30). These concentrations give a LHV of 40.84 MJ/Kg, 41.49 MJ/Kg, and 42.14 MJ/Kg, respectively. In the successive, we plot the simulation results for the different types of fuel, so that they are easy to compare visually.

We adopt the following notation in the plots for each type of fuel: we use a □ to denote the pure biodiesel fuel, a ⋆ to denote the B10 fuel, a △ to denote the B20 fuel, a ∗ to denote the B30 fuel, and a ◯ to denote the Jet-A1 fuel.

Figure 11 shows the air pressure through the engine stages for the two different throttle ranges. We clearly observe a pressure rise at the compression section, as well as an expansion process at the turbine stages. It is evident for both operations ranges that the maximum pressure is located at the centrifugal compressor's discharge (stage 2) and that there is a slight loss in this pressure at the burner (stage 3). In the full throttle case (right side of the figure), it can be observed that the pressure gap inside the burner between the Jet-A1 fuel and the pure biodiesel fuel is considerable, with an observable maximum pressure of 750 kPa and a lower pressure of 610 kPa. In the case of the 60% throttle, there is a difference of 60 kPa between those fuels, with a maximum pressure of 460 kPa and a minimum pressure of approximately 400 kPa. The fuel blends give results that lay below some 5% of the Jet-A1 pressure range. In any case, the maximum values of pressure are related to the use of the Jet-A1 fuel. This can be explained since it delivers the highest amount of power, which in turn is extracted by the turbine stage and transferred to the compression section via the engine spool.

Figure 12 displays the air temperature through the engine stages for the two different throttles. The temperature results agree well with those reported in the manual: the maximum air temperature is observed at the burner discharge

Table 5. Simulation results. Stationary temperatures and pressures at different stations of the PT6A-42 engine. The relative error is calculated against the reported results in Table 3.

Station	T (K)	Error (%)	p (pa)	Error (%)
1.5	433.63	4.39	423635.89	37.76
2	510.44	16.38	749710.57	4.78
3	1231.15	1.57	727219.25	5.57
3.5	896.92	7.26	240006.35	2.49
4	719.69	11.31	1111067.77	1.77
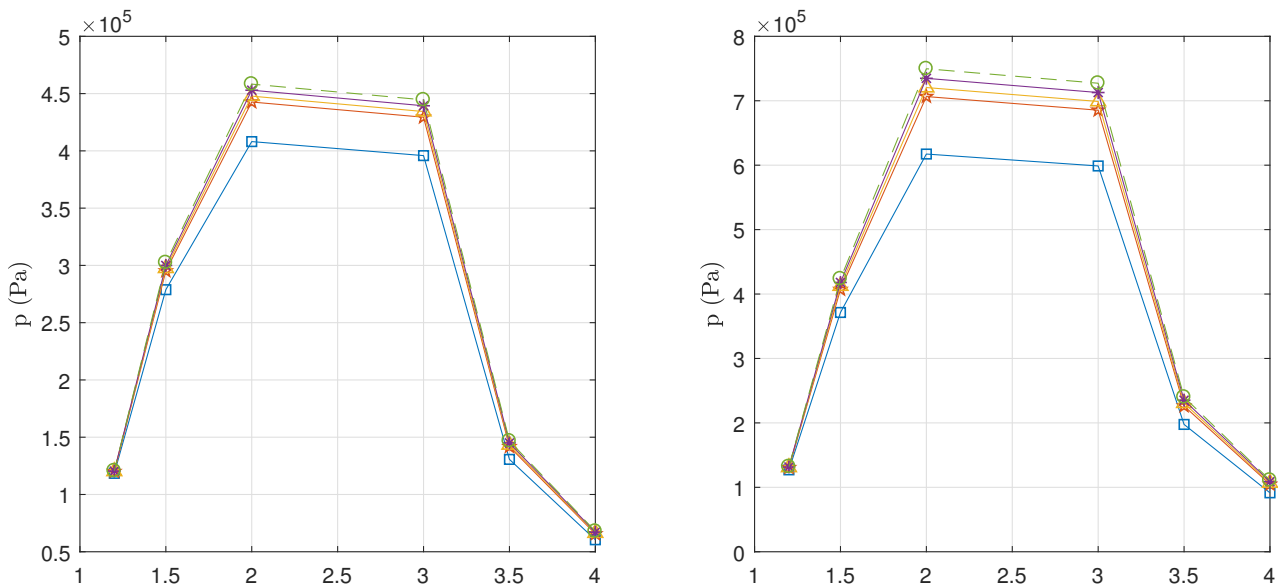
Figure 11. Pressure distribution along the engine stages. Results for the stationary engine operation with the 60% **(left)** and 100% **(right)** throttles.

(stage 3). In any scenario, the fuel that provides the highest temperature to the engine is the Jet-A1 fuel. For the full throttle operation there is a 100 K temperature difference in the burner between the Jet-A1 fuel and the pure biodiesel fuel: the maximum temperature is given for the Jet-A1 fuel, reaching 1230 K, while the minimum temperature of 1140 K is given by the biodiesel operation. The highest drop in temperature occurs at the compression turbine, while the power turbines contribute lesser to the temperature reduction. It is also observed that the temperature difference arising between the fuels at the burner is kept constant at the turbines discharge (stage 4). No important temperature variation is observed for the biodiesel blends. Regardless of the fuel type, the temperature never exceeds a value of 1000 K for the 60% throttle operation.

We also analyze the response of the engine to different loads. We set the full throttle operation and evaluate the rotational speed of the power shaft N_p for several different loads. The results of the conventional operation of the engine using the 5 different types of fuels are presented in Fig. 13, where we observe a diminution in the rotational speed N_p when the load M_l is increased. Nevertheless, this inverse relation is not linear, and therefore we observe a better engine response (shaft power) at the highest loads. It is recognized that the most calorific fuel -the Jet-A1 fuel- gives increased rotational speeds and therefore greater shaft power. On the contrary, the biodiesel operation gives almost 12% less rotational speed than Jet-A1.

Lastly, we present the calculation of the thermal efficiencies of the engine steady operation with the different fuels. This is, we calculate the Brayton's cycle efficiency and the brake efficiency of the engine, being, respectively,

$$\eta_b = \left(1 - \frac{T_4 - T_{atm}}{T_3 - T_2}\right) \qquad \text{and} \qquad \eta_r = \frac{\omega_p M_l}{\dot{m}_f LHV}. \tag{1}$$

We fix a constant load and evaluate the efficiency for several throttles. The efficiency results of the steady operation are presented in Figure 14. We observe that the efficiency curves do not correspond to the ones reported in experimental setups, where the efficiency grows linearly with the fuel mass flow, reaching a plateau where the maximum efficiency is located and finally decreasing. In the present results, both efficiency curves decrease being strongly coupled with the amount of fuel mass flow: the amount of delivered power increases with the fuel flow, but the extracted mechanical power at the turbine stages remains almost constant. Still, the thermal efficiencies at full throttle correspond well to the reported stationary efficiencies of the PT6A-42 engine, with the best efficiency record given by the biodiesel fuel. The efficiency decreases with the concentration of biodiesel in the Jet-A1 fuel, having the conventional operation with the Jet-A1 fuel the lowest efficiency. Even though we recognize a spurious behavior in the efficiency curve that can be explained by an excess of air flowing through the turbine stages, the higher efficiencies reported for blends of biodiesel
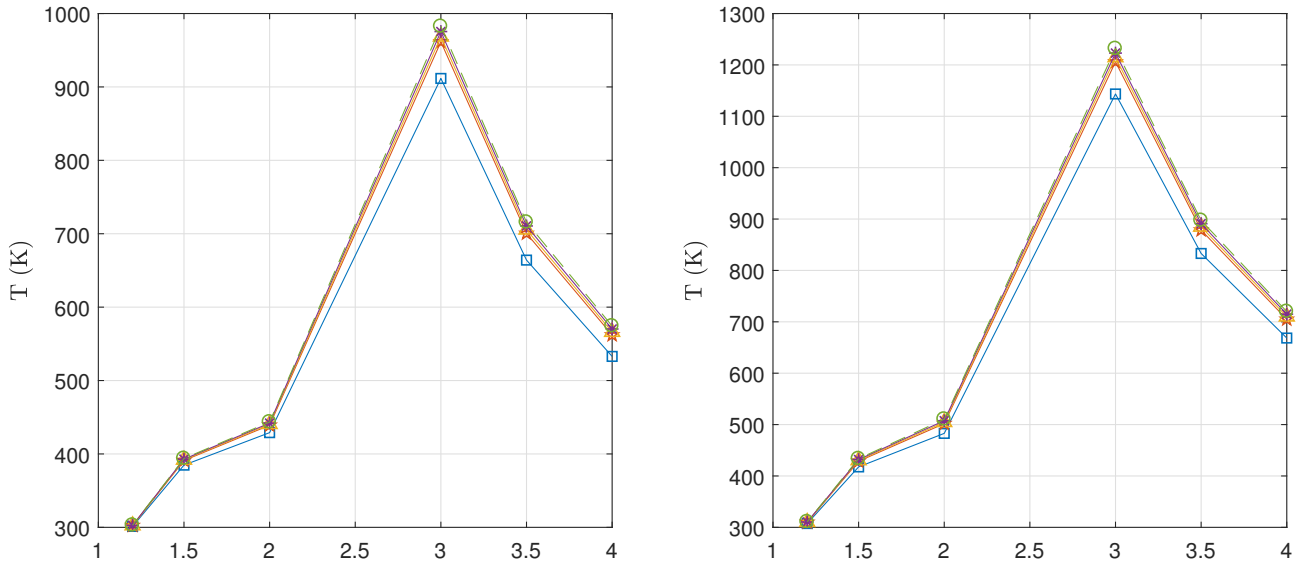
Figure 12. Temperature distribution along the engine stages. Results for the stationary engine operation with the 60% **(left)** and 100% **(right)** throttles.
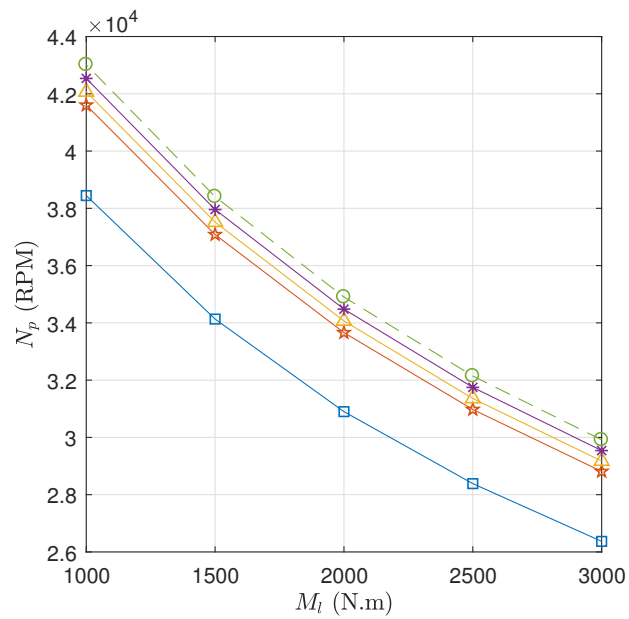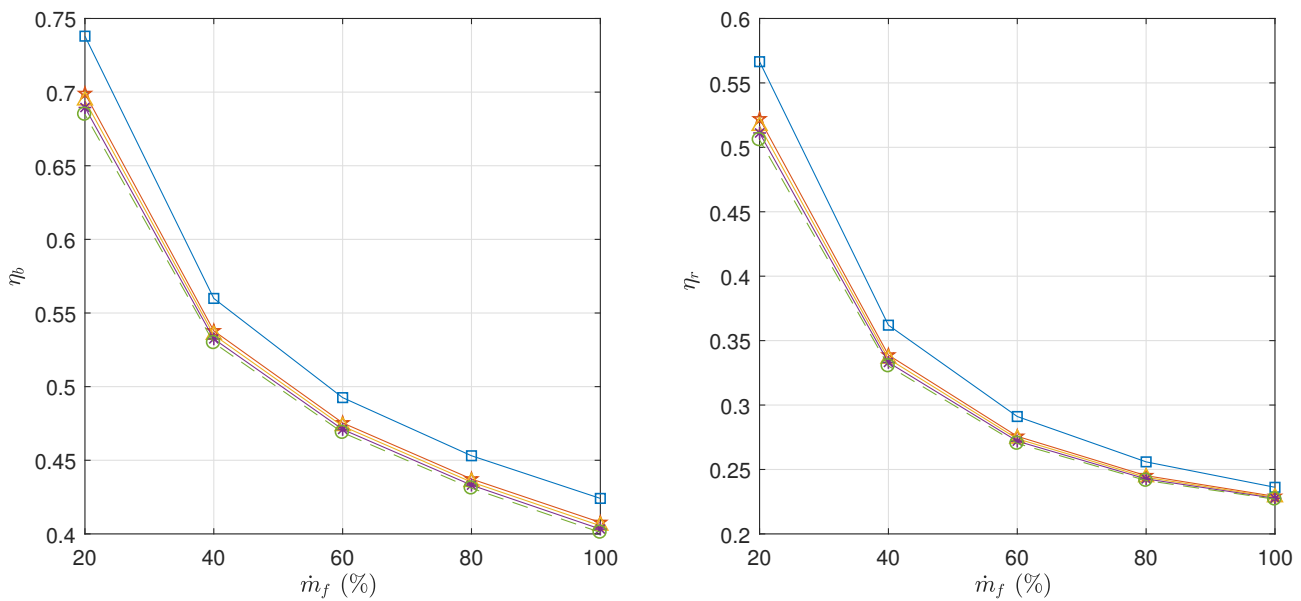

Figure 13. Rotational speed of the power shaft. Results for different loads.

Figure 14. Efficiency results. Thermal efficiency **(left)** and brake efficiency **(right)** for the engine operation with different throttles.

are promissory. Also, the combustion control -which has been neglected in the present model- may help to explain the difference between the present results and the experimental ones, since it reduces the amount of fuel entering the engine when the air flowing through the engine stages is not sufficient to perform stoichiometric combustion.

3.3. Transient operation of the PT6A motor using fuel blends

Finally, we evaluate the start-up procedure of the engine with the fuel types that have been tested in previous scenarios. The main goal is to identify problematic conditions during the engine start-up, which is the transient procedure that can actually affect the engine's integrity. For reproducing the start-up scenario, we initialize the engine spool to an angular velocity of $N_c(t = 0) = 12000$ RPM, that is the rotational speed that is provided by the starter. From this point, there is a positive increment of the air pressure (given by the rotation of the compression system) until the desired mass flow of air into the burner is granted. During the initial compression operation, no fuel mass flow is injected into the burner. We consider that at a later instant $(t = 10)$ s, when the compressed air into the burner stabilizes, the fuel is injected into the burner and ignited. The mass fuel flow is then gradually increased until the desired throttle is reached at $(t = t_f)$. All the start-up procedure is considered to undergo with a constant load.

We aim to evaluate the start-up procedure of the PT6A-42 engine with both 100% and 60% of throttle. The results for the operation with fuel blends are displayed similarly as for the stationary operation. We present comparisons of some important variables, such as the air pressure at the compressor discharge and the air temperature inside the burner. It is noticeable that the start-up procedure converges to the steady-state operation.

Figure 15 shows the transient pressure results at the compression stage for the two different throttles. It can be observed that the pressure in the compressor's discharge undergoes an initial equilibrium when the engine spool is started, reaching a compression ratio below of 1.5 : 1 atm. At $(t = 10)$ s, when the fuel is ignited, a sudden increment of the compression ratio of around 2 : 1 atm is noticed for all fuels and throttles. In the case of the 60% throttle, the pressure stabilizes from this instantaneous peak, but the pressure keeps increasing for the full throttle case reaching the reported 8 : 1 atm compression ratio. There is not a significant pressure fluctuation related to the fuel blends: it can only be appreciated a moderate increment for the full throttle and the biodiesel fuel than for the blends and Jet-A1 fuel.

The transient temperature inside the burner is presented in Figure 16 for the two different throttles. We observe a slight increment in the temperature at the initial compression operation. Then, the fuel intake generates a temperature peak in the combustion chamber, which in all scenarios is the maximum temperature that is reached throughout the operation of the engine. Since the initial fuel flow is the same for both throttle scenarios, the maximum temperature in
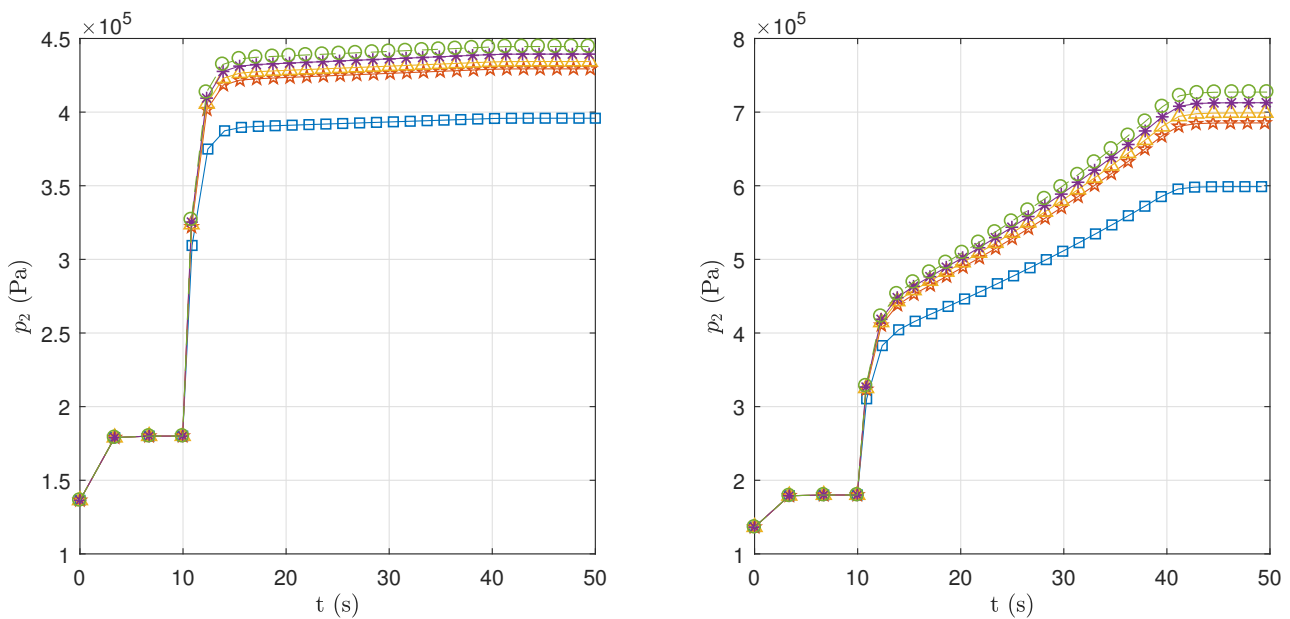
Figure 15. Transient pressure at the compressor's discharge. Results for the start-up operation with the 60% **(left)** and 100% **(right)** throttles.

the engine does not vary. Instead, it only depends on the fuel blend, where the maximum temperature of 1220 K inside the burner is obtained with the Jet-A1 fuel, and the minimum of 1100 K, approximately, is obtained with the pure biodiesel. After this critical instant, the temperature stabilizes at around 1000 K for the 60% case, with a fluctuation of less than 100 K between the blends and the biodiesel fuel. On the other hand, the temperature in the full throttle scenario increases gradually until the steady state of 1200K is reached at about 40 s.

4. Conclusions

In this article, we have simulated the PT6A engine operating at off-design conditions. For this, we have simplified the PT6A engine in a process that extracted the essential components of the engine and eliminated the auxiliary ones. The mass, linear momentum, angular momentum, and energy balances have been applied into these components, by which together with the compatibility conditions compose a 0-dimensional thermo-fluidic model of the engine. We have implemented the numerical solution of the model in the SIMULINK software and different simulation scenarios have granted the predictive capacity of our computational model in relation to the systemic response of the engine. Firstly, we have performed a comparison of some thermodynamic variables against the ones reported in the PT6A-42 manual. The distribution of temperatures and pressures through each of the engine stages shows similar behavior to that predicted in the thermodynamic theory, as well as in the previously reported experimental measurements of the engine. The relative error between the present results and those reported in the manual is below 10% for most of the stages.

The evaluation of the engine response against the change in the composition of the fuel has been achieved next: on one side, to test the hypothetical operation of the engine with blends of biodiesel, but also to predict the start-up response of the engine, which is a complex and transient phenomenon that depends greatly on the type of fuel. In the transient engine starting procedure, the air inside the chamber reaches a temperature peak at the moment of fuel ignition, and the ratio of this temperature to the fuel type is crucial. The simulation results allow us to conclude that the use of blends of biodiesel that are less energetic than the conventional Jet-A1 fuel would not generate a burner overheating since the standard temperature of 1220 K inside the chamber is never exceeded. It is also clear that fuel blends would not generate a pressure excess in the compressor's discharge, and consequently, these can not generate internal damage to the motor structure. We have also observed that the thermodynamic efficiencies are closely related to the amount of air flowing through the power turbines, as well as to the hypothetical fuel heating value: higher
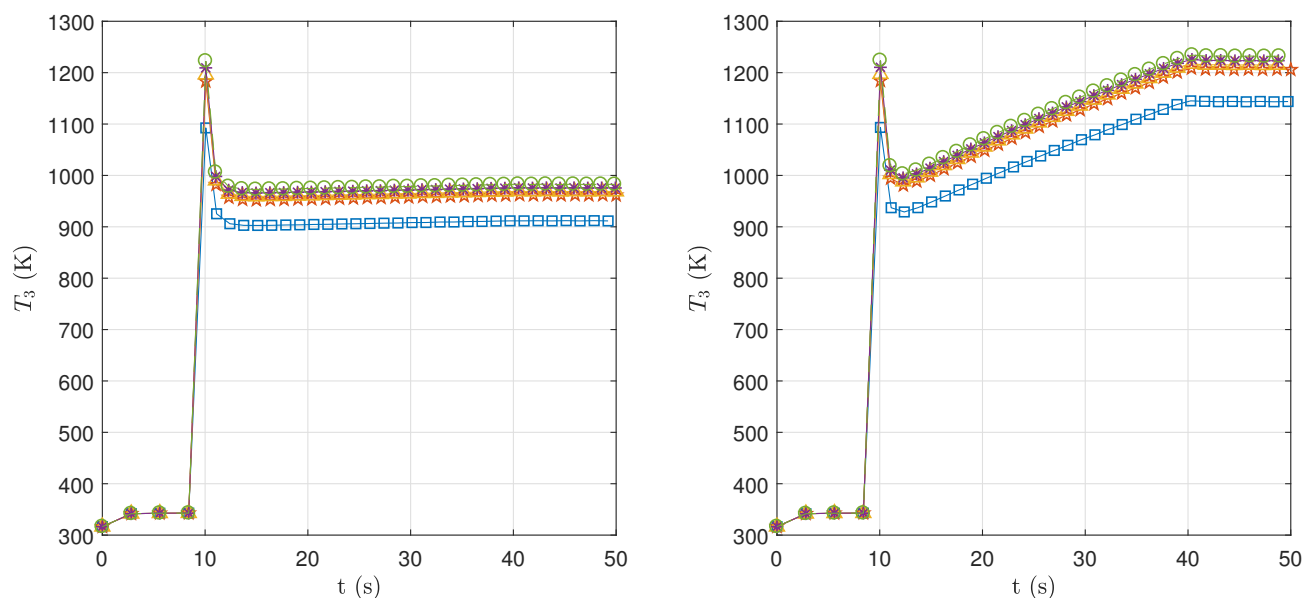
Figure 16. Transient temperature at the burner. Results for the start-up operation with the 60% **(left)** and 100% **(right)** throttles.

efficiencies are found for the engine operation with fuel blends, giving promissory results of the hypothetical PT6A-42 operation with these type of fuels.

As a future work, kinetic combustion models can be coupled to the present model in order to determine the added heat and the production of gases. It is also possible to implement engine control: torque control, pressure control, but especially, combustion control.

Acknowledgments

References

1.   Kong, C.; Ki, J.; Koh, K.   Steady-State and Transient Performance Simulation of a Turboshaft Engine with Free Power Turbine.   ASME 1999 International Gas Turbine and Aeroengine Congress and Exhibition. Citeseer, 1999, pp. V002T04A016–V002T04A016.

2.   Kong, C.; Roh, H. Steady-state Performance Simulation of PT6A-62 Turboprop Engine Using SIMULINK®. *International Journal of Turbo and Jet Engines*, *20*, 183–194.

3.   Alexiou, A.; Mathioudakis, K. Development of gas turbine performance models using a generic simulation tool. ASME Turbo Expo 2005: Power for Land, Sea, and Air. American Society of Mechanical Engineers, 2005, pp. 185–194.

4.   Cuenot, B. Chapter Four - Gas Turbines and Engine Simulations. In *Thermochemical Process Engineering*; Academic Press, 2016; Vol. 49, *Advances in Chemical Engineering*, pp. 273 – 385. doi:https://doi.org/10.1016/bs.ache.2016.09.004.

5.   Menon, S. Simulation of Combustion Dynamics in Gas Turbine Engines. In *Parallel Computational Fluid Dynamics 2002*; North-Holland: Amsterdam, 2003; pp. 33 – 42. doi:https://doi.org/10.1016/B978-044450680-1/50005-X.

6.   Singh, R.; Maity, A.; Nataraj, P. Modeling, Simulation and Validation of Mini SR-30 Gas Turbine Engine. *IFAC-PapersOnLine* **2018**, *51*, 554 – 559. 5th IFAC Conference on Advances in Control and Optimization of Dynamical Systems ACODS 2018, doi:https://doi.org/10.1016/j.ifacol.2018.05.093.

7.   Liu, J.; Hussain, S.; Wang, L.; Xie, G.; Sundén, B. Effects of a pocket cavity on heat transfer and flow characteristics of the endwall with a bluff body in a gas turbine engine.   *Applied Thermal Engineering* **2018**, *143*, 935 – 946. doi:https://doi.org/10.1016/j.applthermaleng.2018.08.020.

8. Sousa, J.; Paniagua, G.; Collado-Morata, E. Thermodynamic analysis of a gas turbine engine with a rotating detonation combustor. *Applied Energy* **2017**, *195*, 247 – 256. doi:https://doi.org/10.1016/j.apenergy.2017.03.045.

9. Wang, M.; Chen, Y.; Liu, Q. Experimental study on the gas engine speed control and heating performance of a gas Engine-driven heat pump. *Energy and Buildings* **2018**, *178*, 84 – 93. doi:https://doi.org/10.1016/j.enbuild.2018.08.041.

10. Xia, Z.; Tang, X.; Luan, M.; Zhang, S.; Ma, Z.; Wang, J. Numerical investigation of two-wave collision and wave structure evolution of rotating detonation engine with hollow combustor. *International Journal of Hydrogen Energy* **2018**. doi:https://doi.org/10.1016/j.ijhydene.2018.09.165.

11. Smirnov, N.; Nikitin, V.; Stamov, L.; Mikhalchenko, E.; Tyurenkova, V. Rotating detonation in a ramjet engine three-dimensional modeling. *Aerospace Science and Technology* **2018**, *81*, 213 – 224. doi:https://doi.org/10.1016/j.ast.2018.08.003.

12. Dagaut, P.; Cathonnet, M. The ignition, oxidation, and combustion of kerosene: A review of experimental and kinetic modeling. *Progress in Energy and Combustion Science* **2006**, *32*, 48 – 92. doi:https://doi.org/10.1016/j.pecs.2005.10.003.

13. Nascimento, M.; Lora, E.; Corrêa, P.; Andrade, R.; Rendon, M.; Venturini, O.; Ramirez, G. Biodiesel fuel in diesel micro-turbine engines: Modelling and experimental evaluation. *Energy* **2008**, *33*, 233 – 240. 19th International Conference on Efficiency, Cost, Optimization, Simulation and Environmental Impactof Energy Systems, doi:https://doi.org/10.1016/j.energy.2007.07.014.

14. Azami, M.; Savill, M. Comparative study of alternative biofuels on aircraft engine performance. *Proceedings of the Institution of Mechanical Engineers, Part G: Journal of Aerospace Engineering* **2017**, *231*, 1509–1521, [https://doi.org/10.1177/0954410016654506]. doi:10.1177/0954410016654506.

15. Gatto, E.; Li, Y.; Pilidis, P. Gas turbine off-design performance adaptation using a genetic algorithm. ASME Turbo Expo 2006: Power for Land, Sea, and Air. American Society of Mechanical Engineers, 2006, pp. 551–560.

16. Li, Y.; Ghafir, M.; Wang, L.; Singh, R.; Huang, K.; Feng, X.; Zhang, W. Improved multiple point nonlinear genetic algorithm based performance adaptation using least square method. *Journal of Engineering for Gas Turbines and Power* **2012**, *134*, 031701.

17. Li, Y.; Ghafir, M.; Wang, L.; Singh, R.; Huang, K.; Feng, X. Nonlinear multiple points gas turbine off-design performance adaptation using a genetic algorithm. *Journal of Engineering for Gas Turbines and Power* **2011**, *133*, 071701.

18. Pan, M.; Cao, L.; Zhou, W.; Huang, J.and Chen, Y. Robust decentralized control design for aircraft engines: A fractional type. *Chinese Journal of Aeronautics* **2018**. doi:https://doi.org/10.1016/j.cja.2018.08.004.

19. Zhang, T.; Wu, H.; Fang, Q.; Huang, T.; Gong, Z.; Peng, Y. UHP-SFRC panels subjected to aircraft engine impact: Experiment and numerical simulation. *International Journal of Impact Engineering* **2017**, *109*, 276 – 292. doi:https://doi.org/10.1016/j.ijimpeng.2017.07.012.

20. Balli, O. Advanced exergy analyses of an aircraft turboprop engine (TPE). *Energy* **2017**, *124*, 599 – 612. doi:https://doi.org/10.1016/j.energy.2017.02.121.

21. Sirignano, W.; Liu, F. Performance increases for gas-turbine engines through combustion inside the turbine. *Journal of propulsion and power* **1999**, *15*, 111–118.

22. Liu, F.; Sirignano, W. Turbojet and turbofan engine performance increases through turbine burners. *Journal of propulsion and power* **2001**, *17*, 695–705.

23. Ghoreyshi, S.; Schobeiri, M. Numerical simulation of the multistage ultra-high efficiency gas turbine engine, UHEGT. ASME Turbo Expo 2017: Turbomachinery Technical Conference and Exposition. American Society of Mechanical Engineers, 2017, pp. V003T06A034–V003T06A034.

24. MATLAB Simulink Toolbox, Release 2016a.

25. Whitney, P.. *PT6 TRAINING MANUAL*; Canada, 2001.

26. Yoshinaka, T.; Thue, K. A Cost-Effective Performance Development of the PT6A-65 Turboprop Compressor. ASME 1985 Beijing International Gas Turbine Symposium and Exposition. Citeseer, 1985, pp. V001T02A015–V001T02A015.

27. Cheng, T.; Simone, H. Measurements of laminar flame speeds of liquid fuels: Jet-A1, diesel, palm methyl esters and blends using particle imaging velocimetry (PIV). *Proceedings of the Combustion Institute* **2011**, *33*, 979 – 986. doi:https://doi.org/10.1016/j.proci.2010.05.106.

28. Llamas-Lois, A. Biodiesel and biokerosenes: Production, characterization, soot & pah emissions. PhD thesis, ETSI_Energia, 2015.